Dynamic Light Scattering Studies on Network Formation of Bridged Polysilsesquioxanes Catalyzed by Polyoxometalates

Yusuke Aoki, Tomohisa Norisuye,* and Qui Tran-Cong-Miyata

Department of Polymer Science and Engineering, Kyoto Institute of Technology, Matsugasaki, Sakyo-ku, Kyoto 606-8585, Japan

Shigeki Nomura and Toshiya Sugimoto

R&D and Technology Center, Sekisui Chemical Co., Ltd., 2-1 Hyakuyama, Shimamoto-cho, Mishima-gun, Osaka 618-8589, Japan

Received July 14, 2003; Revised Manuscript Received October 28, 2003

ABSTRACT: The sol−gel process of 1,8-bis(triethoxysilyl)octane (TES-Oct) catalyzed by phosphotungstic acid (PWA) has been investigated by time-resolved dynamic light scattering. The time−intensity correlation functions (ICF) exhibited two modes, corresponding to the cooperative diffusion of entangled chains and the translational diffusion of cross-linked clusters. Below the gelation threshold the ICFs were well described by sum of two exponential functions, allowing the successful analysis of the relaxation times and the corresponding relative intensity for the fast and slow modes. On the contrary to general observation of acid-catalyzed systems, the specific gelation process was found for $r_{PWA} = 0.100$, the molar ratio of PWA to TES-Oct. Namely, the relative amplitude for the fast relaxation, A_f, and the averaged slow relaxation time, $\langle\tau_{slow}\rangle$, exhibit exceptionally larger values in the gelation process, suggesting the existence of the ionized larger clusters as found for the base-catalyzed system. The hydrodynamic radii, R_H, were also evaluated by dilution of the gel forming samples at several sampling points in order to confirm the existence of the larger cluster during gelation. In addition to the normal increase in R_H in the sol−gel process, it was found that the matrix viscosity and/or hydrodynamic interaction play a significant role in both the slow dynamics, e.g., divergence of $\langle\tau_{slow}\rangle$ in the gelation process and a power law behavior in the ICF around gelation threshold, in this system.

Introduction

Bridged polysilsesquioxanes are a family of organic−inorganic polymer hybrids composed of siloxane units bridged by variable organic groups.[1−4] These materials exhibit favorable structural rigidity and organic functionality owing to their unique structure at a molecular level. The ease of their preparation as well as their excellent physical and chemical properties led to potential applications such as optical devices, catalyst supports, electronic devices, fuel cells, and so on. For example, proton conductive membranes can be synthesized by sol−gel reaction of alkoxysilanes with organic bridges, such as ethylene oxide, propylene oxide,[5,6] and isocyanatopropylene oxide,[7] in the presence of phosphotungstic acid (PWA). PWA belongs to a large group of oxometalate[8,9] and has an exceptional high conductivity.[10] Although the PWA-dispersed membrane can be considered as a good candidate for such applications, the conductivity strongly depends on the structure of the silica network and the spatial distribution of PWA, in addition to the state of water molecules around PWA. Electrolyte dispersed polymer composites have been prepared and extensively studied by small-angle X-ray (SAXS) and neutron scattering (SANS),[5,11] Fourier transform infrared spectroscopy (FTIR),[7] and X-ray diffraction (XRD) techniques. SAXS has been employed in order to characterize the microscopic structure, whereas FTIR and XRD have been used to confirm the preservation and the immobilization of PWA. Needless to say, the crystallization and the phase separation must be circumvented. Therefore, designing conductive membrane is focused on the exploration of the homogeneous network structure and random distribution of the proton conductor with maximum amount of PWA.

Dynamic light scattering (DLS) is a powerful tool to characterize the structure and dynamics for polymer solutions with micelles or aggeregates,[12,13] gels,[14−18] proteins,[19,20] and bulk copolymer.[21] Because of several advantages, such as short accession time and suitable length scale for polymer cluster investigation, DLS has been further developed for studying in situ the time-dependent experiments of polymerization, protein aggregation, gelation, and vitrification. In our previous studies, we demonstrated that the acid- and base-catalyzed sol−gel process of tetramethoxysilane can be monitored by time-resolved dynamic light scattering (TRDLS).[22] These results indicate that the long siloxane strands with less branching point were formed by the acid-catalyzed gelation, whereas the larger clusters with highly branched points were formed by the base catalyst in the early stage of sol−gel reaction followed by rather slow kinetics due to intercluster repulsion. Since the TRDLS is suitable for investigation of growing clusters, we applied the technique to monitor in situ the networking process of polymer composites consisting of alkylene-bridged polysilsesquioxane and PWA. To further understand the slow mode of ICF which appeared in the gelation process, the reacting samples were diluted at several sampling points and were investigated by DLS as a function of the concentration and the scattering angle. The obtained relaxation times or the corresponding hydrodynamic radius, R_H, was compared to that of the reacting samples without dilution. Finally, the gelation mechanism and the correlation between the

* To whom correspondence should be addressed.

10.1021/ma034987b CCC: $25.00 © 2003 American Chemical Society
Published on Web 12/03/2003

conductivity and the structure will be discussed on the basis of the time course of the cluster size and the hydrodynamic interactions between clusters during the sol−gel process.

Experimental Section

Samples. Sol−gel precursor, 1,8-bis(triethoxysilyl)octane (TES-Oct; Gelest), $(OC_2H_5)_3-Si-(CH_2)_8-Si-(OC_2H_5)_3$, and phosphotungstic acid (PWA; Aldrich), $H_3PW_{12}O_{40}\cdot nH_2O$, were mixed in 2-propanol (IPA; Wakenyaku), where n indicated the hydrated water in PWA. Note that PWA plays a role not only as a proton conductor in the PWA dispersed membrane but also as a strong acid catalyst in the reaction. It contains usually 29 hydrated water molecules at ambient temperature, but 6-bound water is left for the higher temperature. The existence of several phases under a given temperature, pressure, and humidity was discussed in the literature.[23] Therefore, in this study, PWA was once dried in vacuo at 50 °C until its weight becomes a constant. Then the prescribed amount of water with stoichiometric ratio $[H_2O]/[-OC_2H_5] = 0.5$ was added to the PWA/IPA solution. The effects of drying on the microscopic structure of the polymer composites are addressed elsewhere.[24] The concentration of PWA was adjusted with a fixed the molar ratio of PWA to TES-Oct, $r_{PWA} = 0.025$, 0.050, 0.067, 0.080, 0.090, 0.100, 0.125, 0.135, and 0.150. For comparison, the acid-catalyzed TES-Oct sample in the absence of PWA ($r_{PWA} = 0$) was prepared with 1 N hydrochloric acid (HCl; Wakenyaku). The concentration of TES-Oct was kept at 18.67%. The reaction batch was prepared by adding a mixture (PWA + water + IPA) into another mixture (TES-Oct + IPA) to initiate the reaction. After vigorous stirring, the solution was filtered through a Teflon membrane of pore size 0.25 μm and poured into a purified test tube.

Dynamic Light Scattering. Dynamic light scattering measurements were carried out on two types of apparatus. For time-resolved dynamic light scattering (TRDLS) measurements, a DLS/SLS-5000 multitau photon correlator system (ALV, Langen) coupled with a vertically polarized 632.8 nm line of a He−Ne laser (Uniphase; 22 mW) was employed to ensure a wide range of sampling for the log time. Scattering intensity data from the reactor batch were collected for every 60 s as a function of t at the fixed scattering angle of 90° at 30 °C.

For subsequent particle sizing, the reaction was quenched by dilution with a large amount of solvents. The relaxation of cross-linking clusters became faster than that for reaction batch and exhibited rather monotonic decay. To evaluate the faster decay, the relaxation data obtained in the short time scale were collected with 1024 channels by a DLS7000 linear photon correlator system (Otsuka Electric Co., Japan) using an Ar laser (NEC, 75 mW) as a light source. The sampling time was set to an optimum value to obtain a fully decaying ICF, which is typically 4 μs. The correlation functions were recorded in the angular range 30°−150° at appropriate dilution at 30 °C. The experimental temperature was thermostated within a temperature range ±0.1 °C.

Data Analysis

Dynamic Light Scattering.[25,26] The time-averaged intensity, $\langle I(q,t)\rangle_T$, and its intensity−intensity correlation functions, $g_T^{(2)}(q,t)$, expressed by

$$g_T^{(2)}(q,t) \equiv \frac{\langle I(q,0)\, I(q,t)\rangle_T}{\langle I(q,0)\rangle_T^{\,2}} = 1 + |g^{(1)}(q,t)|^2 \qquad (1)$$

are obtained by DLS, where $\langle ...\rangle_T$ denotes the time average and q is the magnitude of the scattering wave vector. $g^{(1)}(q,t)$ is the scattering field time-correlation function given by

$$g^{(1)}(q,t) = \int G(q,\tau)\exp(-t/\tau)\,d\tau \qquad (2)$$

where τ is the relaxation time and $G(q,\tau)$ is the characteristic decay time distribution function. For semidilute or concentrated polymer solutions, two relaxation modes[27,28] corresponding respectively to the cooperative diffusion and the viscoelastic relaxation[29−31] or the large-scale heterogeneities have been reported in the literature. This relaxation behavior strongly depends on the solvent quality, the molecular weight, the observed scattering angle, and so on.[30] The following equation may be applicable to fit the experimental data by taking into account the fact that the slow mode has long time tail distribution[22,32]

$$g_T^{(2)}(q,t) - 1 = \sigma_I^{\,2}[A_f \exp(-t/\tau_f) + A_s \exp\{-(t/\tau_s)^{\beta}\}]^2 \qquad (3)$$

Here, τ_f is the fast relaxation time, $\sigma_I^{\,2}$ is the initial amplitude of the intensity correlation function, and

$$\langle \tau_{slow}\rangle = \frac{\tau_s}{\beta}\Gamma\left(\frac{1}{\beta}\right) \qquad (4)$$

is the arithmetic averaged slow relaxation time, where $\Gamma(x)$ is the gamma function of x. Note that the value of $\sigma_I^{\,2}$ is below unity for the initial stage of the reaction because there is a large amount of solvents and unreacted monomers, which do not contribute to the time correlation but affects the total intensities. Once polymeric gels or glass are formed, $\sigma_I^{\,2}$ also reduces from unity due to the existence of static inhomogeneities. Therefore, it should be noted that the value of $\sigma_I^{\,2}$ less than unity has different physical meanings for before and after gelation threshold. As the polymerization proceeds, the value of $\langle \tau_{slow}\rangle$ and the polydispersity of the relaxation time become larger, resulting in a small β. Instead of eq 3, the ICF becomes a power-law function expressed by[33]

$$g_T^{(2)}(q,t) - 1 = \sigma_I^{\,2}[A_f \exp(-t/\tau_f) + A_s(1 + t/t^*)^{(\alpha-1)/2}]^2 \qquad (5)$$

Here α and t^* are respectively the critical exponent and the lower cutoff of the power-law behavior. This equation well reproduces the experimental data around the gelation threshold for various gelling systems.[22,34−36] Although the theoretical treatment for the value of α has been in controversy, the relation between its values and the network structures are extensively discussed elsewhere.[29,37,38]

The size of clusters was examined by measuring ICF of the reacted samples in order to separate the information of individual clusters from the dynamics of the reactor batch. After a moderate dilution, the arithmetic averaged decay rate may be evaluated by using the slope of the semilogarithmic plot of the correlation functions, i.e.

$$\langle \tau_0^{\,-1}\rangle = -\frac{1}{2}\left[\frac{\partial}{\partial t}\ln\{g^{(2)}(t) - 1\}\right] \qquad (6)$$

For the particle with the size much smaller than q^{-1}, the following relation holds:

$$\langle \tau_0^{\,-1}\rangle = \langle D_{app}\rangle q^2 = \langle D\rangle q^2(1 + \langle k_D\rangle c + ...) \qquad (7)$$

where $\langle D_{app}\rangle$, $\langle D\rangle$, and $\langle k_D\rangle$ are respectively the apparent diffusion coefficient, the z-averaged translational diffusion coefficient, and the proportional constant including

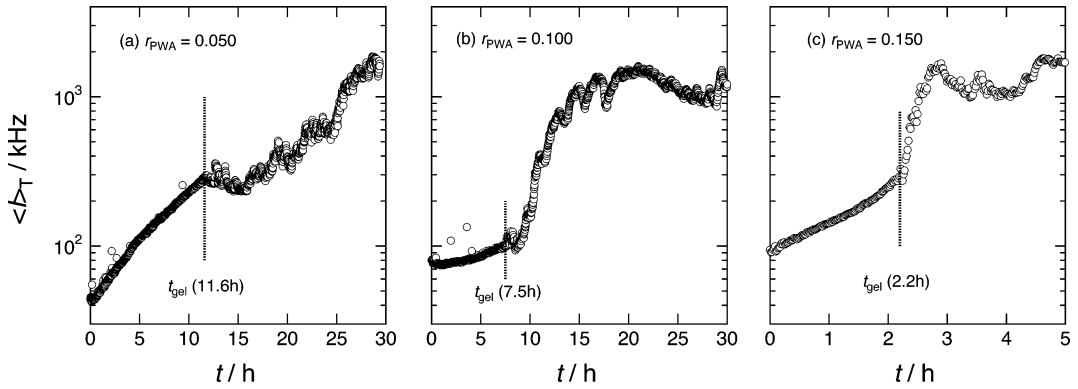

Figure 1. Variation of the scattering intensity of TES-Oct during the gelation process with (a) $r_{PWA} = 0.050$, (b) 0.100, and (c) 0.150. $\langle I \rangle_T$ denotes the time-averaged scattering intensity observed at a fixed scattering angle of 90°. The dotted line indicated the gelation threshold, t_{gel}.

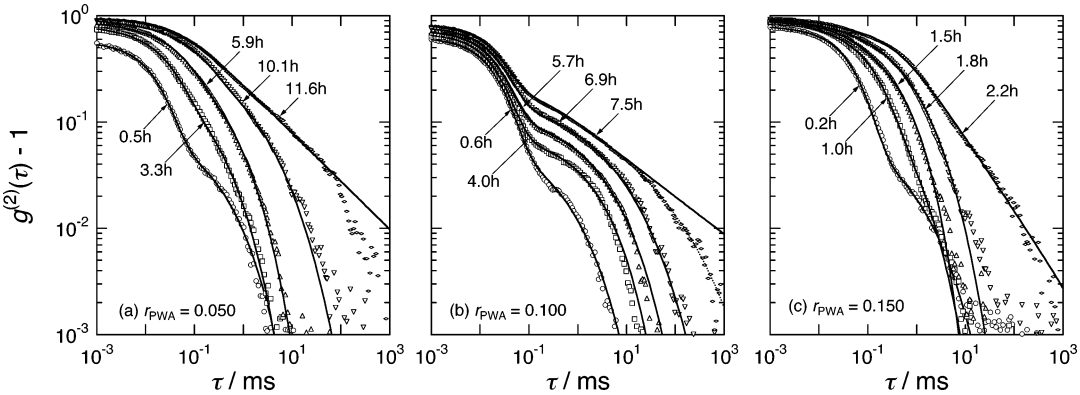

Figure 2. Double-logarithmic plots of the ICFs obtained by DLS during the gelation process for various PWA concentrations. The solid lines indicate the fit with eq 3 or 5.

both the excluded-volume and the hydrodynamic interactions. First, $\langle D_{app} \rangle$ was evaluated from the slope of $\langle \tau_0^{-1} \rangle$ vs q^2 plot. Then $\langle D \rangle$ was obtained by extrapolating $\langle D_{app} \rangle$ to infinite dilution. The hydrodynamic radius, R_H, of the clusters was finally estimated from the Stokes–Einstein relation

$$R_H = \frac{k_B T}{6\pi\eta\langle D \rangle} \tag{8}$$

The time courses of the relaxation time during the gelation process for the reaction batch solutions and the dilute solutions are compared in the following section.

Results and Discussion

In-Situ DLS Analysis. Figure 1 shows the dependence of the scattering intensity on the molar ratio of PWA to TES-Oct during gelation process with (a) $r_{PWA} = 0.050$, (b) 0.100, and (c) 0.150. Here $\langle I \rangle_T$ denotes the time-averaged scattering intensity observed at the fixed scattering angle 90°. A stepwise increasing and subsequent strong fluctuations in $\langle I \rangle_T$[39] were observed for the all PWA concentrations. The fluctuations are ascribed to an emergence of restricted ergodicity, the inherent property of polymeric gels. Thus, the boundary indicated by the dotted line can be regarded as the gelation threshold, t_{gel}. It is further confirmed by the appearance of a power law behavior and the reduction of the initial amplitude of ICF as discussed later. Similar phenomena were observed for various gelling systems, e.g., *N*-isopropylacrylamide gels,[39] methyl methacrylate gels,[35] silica gels with acid and basic catalyst,[22] fibrin gels,[36] and so on. Although the intensities include both the contributions from the cooperative nature of semidilute solutions and the translational diffusion of the cross-linking clusters, we will separate these contributions as described below.

Figure 2 shows the double-logarithmic plots of ICFs during the gelation process for various PWA concentrations. At the beginning, the scattering intensity was too low to construct ICF. As the gelation proceeds, ICFs exhibit two distinct modes, corresponding to the cooperative diffusion in a semidilute solution and the translational diffusion of cross-linked clusters in a concentrated matrix. The slow mode shifts to the side of longer time and finally exhibits a power law behavior around the gelation threshold, t_{gel}. As indicated by the solid lines, the ICFs were well fitted to the combined functions of a single and a stretched exponential function given by eq 3 for $t < t_{gel}$ or a single and power-law function given by eq 5 for $t = t_{gel}$. Although the slow relaxation time was the largest around $t = 7.5$ h, the complete power-law behavior was not observed for $r_{PWA} = 0.100$. As shown by the dotted line, the following power law with an exponential cutoff function seemed to fit well the experimental data:[40]

$$g_T^{(2)}(q,t) - 1 = \sigma_I^2[A_f \exp(-t/\tau_f) + A_s(1 + t/t^*)^{(\alpha-1)/2} \exp(-(t/\tau_{max})^{\beta})]^2 \tag{9}$$

The existence of distinctive cutoff in finite relaxation time may suggest the uniform gelation with a characteristic length scale for $r_{PWA} = 0.100$. It is clear from the figure that with $r_{PWA} = 0.100$ the contribution of the fast mode to the whole ICF decay is larger than other r_{PWA}.

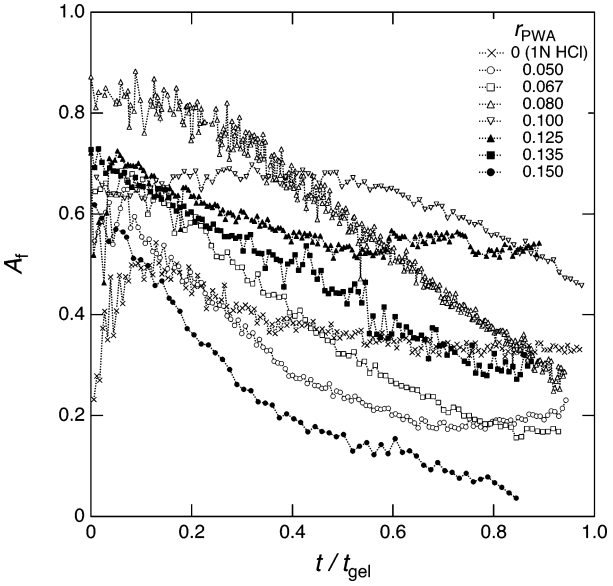

Figure 3. Variation of the relative amplitude of the fast mode, A_f, with the reduced time t/t_{gel}. A_f for $r_{PWA} = 0.100$ exhibited an exceptionally high value among others through the gelation process, suggesting the existence of a repulsive interaction between ionized clusters resembling the base-catalyzed system.

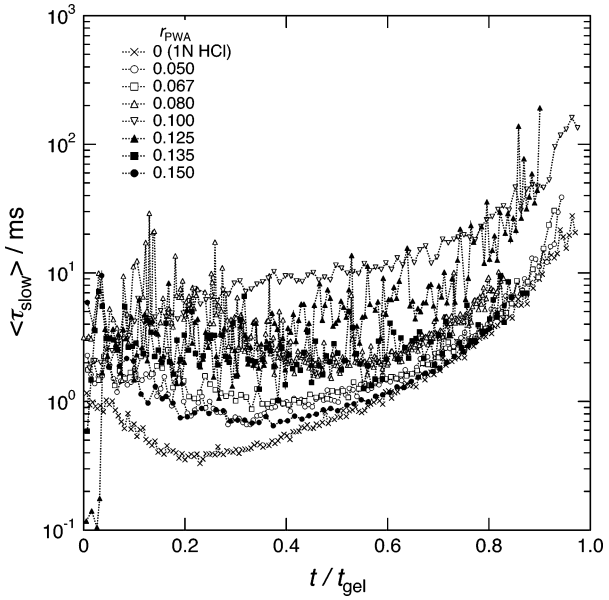

Figure 4. Variation of the slow relaxation time $\langle\tau_{slow}\rangle$ with the normalized reduced polymerization time, t/t_{gel}, for various r_{PWA}s.

The variations of A_f during gelation are illustrated as a function of r_{PWA} in Figure 3 where the abscissa is normalized by gelation time, t_{gel}. A_f was found to decrease with the reduced reaction time for all the r_{PWA}s, suggesting the successful evolution of the cross-linking clusters. On the other hand, A_f at various polymerization times exhibited significantly larger values around $r_{PWA} = 0.080-0.125$. Note that the intensity of the fast mode, assigned to the thermal fluctuations of semidilute solutions, is proportional to the osmotic compressibility and is strongly dependent on the solvent quality as well as the amount of the effective charge, while the slow mode related to the elastic modulus is rather invariant with the solvent quality.[30] Therefore, the characteristic behavior of A_f obtained by DLS may be attributed to the synthetic mechanism accompanied by the catalytic reaction and the state of the clusters with dissociated silanol groups.

It is well-known that the gelation of an acid-catalyzed silica system bears a resemblance to bifunctional alkoxysilane despite four reactive alkoxy groups of alkoxysilane.[41] This is due to the greater ease of protonation for less hydrolyzed alkoxysilane than fully hydrolyzed one. These characteristics of the electrophilic reaction lead to more extended and less branched structure for the acid-catalyzed system. For the lower amount of PWA, e.g., $r_{PWA} = 0.050$, the gelation kinetics observed by TRDLS was quite similar to the common acid catalysts. For example, a decrease of A_f and subsequent gelation with low A_f were observed with 1 N HCl. This observation is consistent with our previous finding for TMOS gelation.[22] On the contrary, for the base-catalyzed system, nucleophilic reagent bearing hydroxyl ion promotes highly branched structure due to the mechanism opposite to the acid-catalyzed system. In this case, the fast mode in the ICF dominates the dynamics during the gelation because the solvent quality is extremely improved by highly ionized species as observed by DLS in semidilute solutions.[30]

Interestingly, it was reported that the conjugate base of the acid catalyst has the ability to increasing the coordination of silicon for the strong acid-catalyzed system, resulting in properties similar to basic catalysts.[42] In our case further introduction of PWA anion, e.g., with $r_{PWA} = 0.100$, may lead to the formation of ionized clusters through the hypervalent silicon with a nucleophilic reaction whereby the gelation followed an unique kinetics with a larger value of A_f. In case the PWA concentration is not too high, the coordination of PWA anion may play an effective role on gelation. However, further introduction of PWA will lead the electrostatic screening with a large amount of phosphotungstic anion and oxonium cation in addition to the dissociated silanol groups, resulting in the similar behavior of A_f with low r_{PWA}. Furthermore, the system approaches the phase boundary of TES/PWA/IPA mixtures with increasing of r_{PWA}. In this case, PWA becomes insoluble in the monomer mixtures and uniform gels are no longer formed. Note that the proton conductivity exhibits a maximum value around $r_{PWA} = 0.100$. These results will be published in the forthcoming paper.

Figure 4 shows the variation of the slow relaxation time, $\langle\tau_{slow}\rangle$, as a function of the reduced polymerization time, t/t_{gel}, for various values of r_{PWA}. $\langle\tau_{slow}\rangle$ increases with t/t_{gel} and finally diverged around the gelation threshold. Clearly, $\langle\tau_{slow}\rangle$ for $r_{PWA} = 0.100$ exhibits the larger values compared among others. This may indicate that the larger clusters are formed in the initial stage of reaction, followed by a gradual interconnection of clusters due to the strong repulsion force between ionized clusters. This polymerization process is strongly resembles to that in the base-catalyzed system and is consistent with the above finding.

In Figure 5, (a) the gelation time, t_{gel}, (b) A_f with different t/t_{gel}, and (c) the critical exponent for the time-correlation function, α_{gel}, are presented as a function of r_{PWA}, where the open and closed symbols respectively denote the results for different PWAs and 1 N HCl. The solid lines are drawn for the eyes. As found in Figure 5a, the gelation time was systematically shortened by the addition of PWA. On the other hand, A_f represented convex upward variation for various t/t_{gel} as shown in Figure 5b. For the initial stage of the reaction, say t/t_{gel}

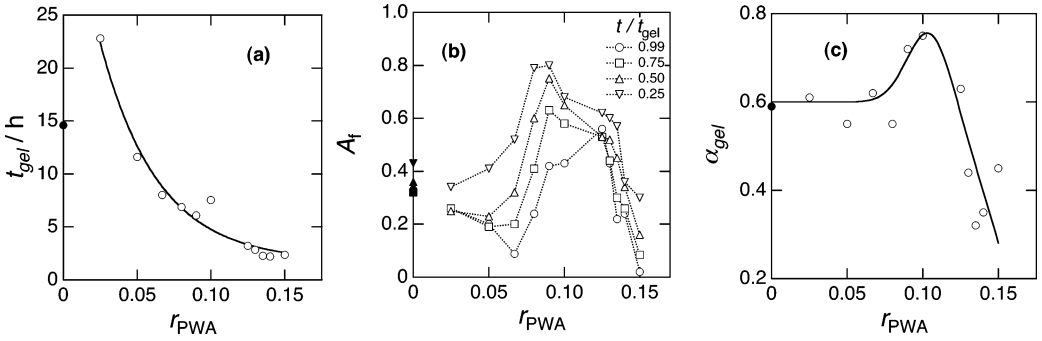

Figure 5. Dependence of (a) t_{gel}, (b) A_f, and (c) α_{gel} as a function of r_{PWA}. The solid lines are drawn for the eyes.

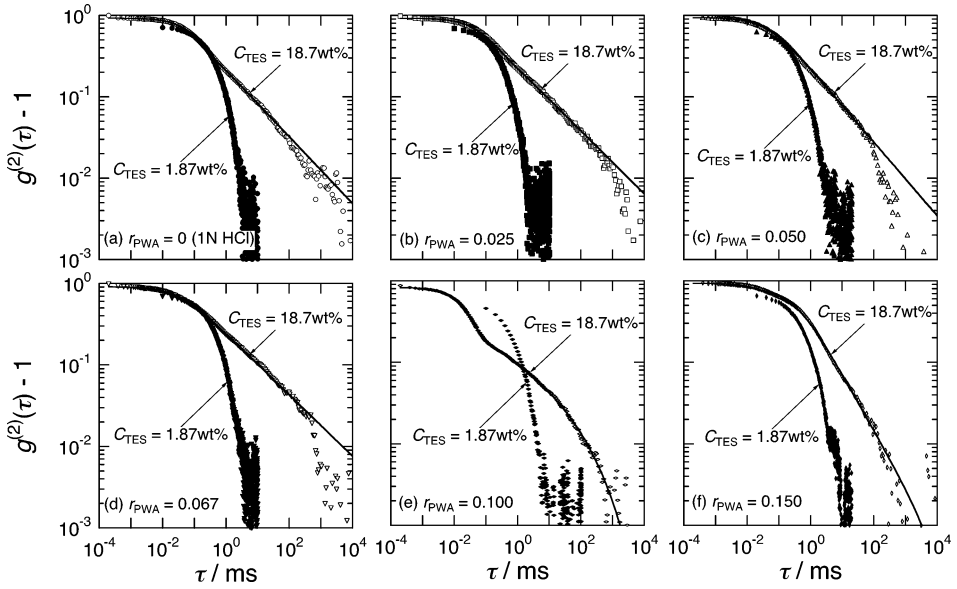

Figure 6. ICFs for various r_{PWA} around gelation threshold. The experimental conditions are indicated by open (batch reaction) and closed (diluted samples) symbols. The power-law behavior disappears when the reacting samples are diluted.

= 0.50, the maximum is located around 0.080. The maximum shifts to the higher r_{PWA}, followed by the final peak location around $r_{PWA} = 0.100$. Although the reason for the shift for the maximum A_f is not clear at this stage, as shown in Figure 5c, the unique kinetics for $r_{PWA} = 0.100$ is also appeared in α_{gel}. It should be noted that the maximum value of α_{gel} is close to the value of 0.84 found for base-catalyzed TMOS.[22]

Cluster Dilution Analysis. We have demonstrated the unique gelation process for 1,8-bis(triethoxysilyl)-octane with $r_{PWA} = 0.100$. However, the details of the reaction mechanism have not been fully elucidated yet. To clarify the problem, the other spectroscopic techniques, such as FTIR and/or ^{29}Si NMR, are strongly desired. However, because of some technical reasons for us, such kinds of experiments are not allowed particularly in situ at this stage. Therefore, we would like to reserve the experiments in the future. Instead, we tried to demonstrate the actual size of the clusters during gelation in this section.

The time evolution of the slow mode and the appearance of the power-law behavior in the ICF are the general characteristics in the gelling system. These phenomena may include an intricate mechanism, such as the viscoelastic coupling[29] and local viscosity associated with the size of the growing clusters. To elucidate this point, the reacting samples taken from the same batch were diluted at several sampling points by an addition of a larger amount of IPA. Again the reaction time was normalized with the gelation time which is determined by the flow test, and the power-law behavior of ICF reappears in measurements using by DLS7000. Figure 6 exhibits ICFs quenched around the gel point by 10-fold dilution (closed symbols) together with that of the reaction batch (open symbols) for various values of r_{PWA}s. As clearly shown in the figure, the power-law behavior disappeared when the reacting samples were diluted. ICF exhibits rather monotonic decay, $\tau_0 \approx 10$ ms, and is well fitted to a stretched exponential function. Similar to the above analysis for the slow relaxation process, the arithmetic averaged relaxation time may be evaluated by eq 4 for the dilute system. On the other hand, the average decay rate, $\langle \tau_0^{-1} \rangle$, which correspond to the inverse of the harmonic averaged relaxation time, is often employed as the standard procedure to calculate the z-averaged diffusion coefficient in dilute solutions.

In Figure 7a, $\langle \tau_0^{-1} \rangle$ is plotted against q^2 for $r_{PWA} = 0.050$ under various reduced time, t/t_{gel}. All the data can be well expressed by straight lines with zero intercept, suggesting that the modes observed under these conditions are diffusive. The slope which corresponds to the apparent diffusion coefficient $\langle D_{app} \rangle$ decreases with the reduced time. Note that the sample just below gelation threshold, $t/t_{gel} = 0.99$, is particularly marked with parentheses in the legend in the figure because of the inaccuracy associated with the rapid solidification. Figure 7b shows the evaluated $\langle D_{app} \rangle$ as a function of C_{TES} for $r_{PWA} = 0.050$ at $t/t_{gel} = 0.75$. $\langle D_{app} \rangle$ decreases with C_{TES} and finally reaches an asymptotic value. Extrapolation of $\langle D_{app} \rangle$ to infinite dilution gives $\langle D \rangle$ of

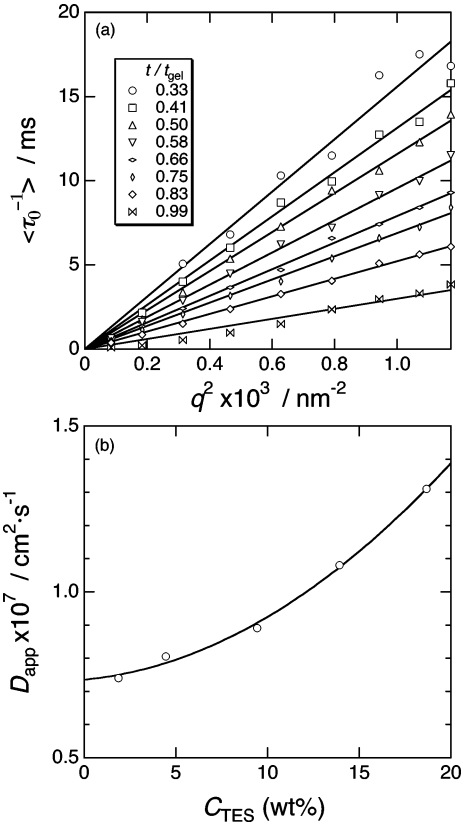

Figure 7. Examples of the data analysis for (a) the angular- and (b) the concentration-dependent experiments: (a) plot of $\langle\tau_0^{-1}\rangle$ vs q^2 for $r_{PWA} = 0.050$ as a function of reduced time. The slope corresponded to the apparent diffusion coefficient, $\langle D_{app}\rangle$. (b) Concentration dependence for $\langle D_{app}\rangle$ for $r_{PWA} = 0.050$ at $t/t_{gel} = 0.75$. $\langle D\rangle$ was obtained by extrapolating $\langle D_{app}\rangle$ to infinite dilution.

7.35×10^{-8} cm^2 s^{-1}, which corresponds to a hydrodynamic radius R_H of 15.0 nm according to the Stokes−Einstein given by eq 12. Although the concentration-dependent experiments were performed under several conditions, hereafter we employed the value at $C_{TES} = 1.87\%$ instead of infinite dilution for convenience. The similar angular-dependent analysis was conducted for the all r_{PWA}s with several sampling points.

Comparison of the time course between the two relaxation process observed in situ and in dilute solutions may provide a better insight into understanding the characteristics of the gelation process. In Figure 8, the time course of the relaxation time observed at the scattering angle of 90° is illustrated for various r_{PWA}s, where open and closed symbols denote $\langle\tau_{slow}\rangle$ and $\langle\tau_0^{-1}\rangle^{-1}$, respectively. As described above, $\langle\tau_{slow}\rangle$ increases as the reaction proceeds and tends to diverge in the vicinity of the gelation threshold. On the other hand, $\langle\tau_0^{-1}\rangle^{-1}$ does not exhibit such a diverging behavior but gradually increases with the growing clusters. The difference between $\langle\tau_{slow}\rangle$ and $\langle\tau_0^{-1}\rangle^{-1}$ becomes significant upon approaching the gelation threshold. Note that the appearance of the nondiverging behavior for the latter is also confirmed for the arithmetic averaged relaxation time evaluated by eq 4. It is deduced from above finding that the size distribution of clusters is not directly related to the power-law behavior of the ICF around the gelation threshold, and the local viscosity correlation may play an important role instead. It is to be noted that the osmotic compressibility may also affect more or less the relaxation time since it is different between before and after dilution. However, in addition to the difference of $\langle\tau_{slow}\rangle$ and $\langle\tau_0^{-1}\rangle^{-1}$ by approaching t_{gel}, disappearance of the power law for ICF suggests the existence of a kind of "correlation" as stated above.

Figure 9 shows the variation of hydrodynamic radius, R_h, calculated by eq 12 as a function of reduced time with various values of r_{PWA}. For all r_{PWA}s, R_h increases due to the growth of clusters during gelation. The growth of clusters with considerably larger size was again confirmed for $r_{PWA} = 0.100$ even under the dilute condition. Therefore, it is concluded that the strong acid, PWA, catalyzed sol−gel processing may proceed in a manner similar to the case of base-catalyzed system; i.e., the reaction takes place with a drastic growth via nucleophilic reaction in the cluster size.

It was deduced from these experimental results that PWA, the strong acid with a moderate concentration (in this case $r_{PWA} = 0.100$), plays the important role of a unique catalyst in controlling the microscopic structure of TES-Oct/PWA solutions as well as its membrane. Since the repulsive interaction of electrolytes tends to

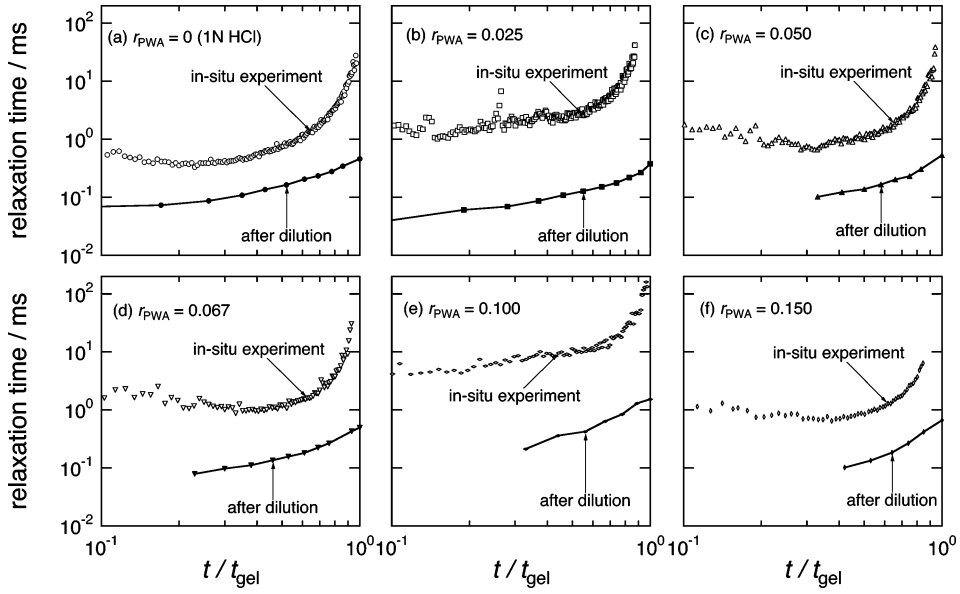

Figure 8. Time course of the relaxation time observed at the scattering angle of 90° for various samples with r_{PWA}s. The open and closed symbols denote $\langle\tau_{slow}\rangle$ and $\langle\tau_0^{-1}\rangle^{-1}$, respectively.

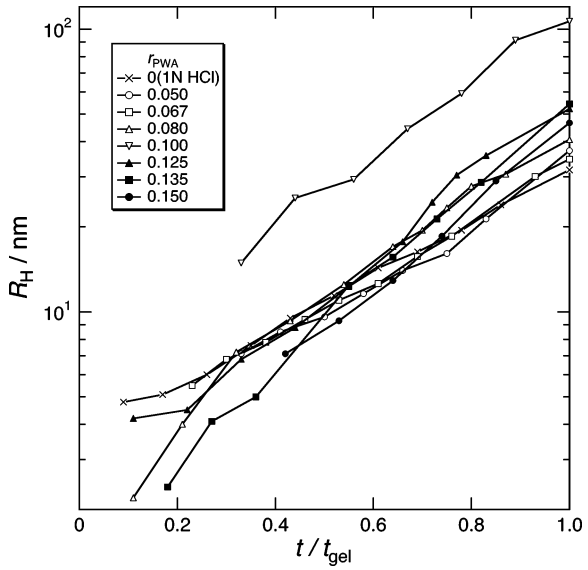

Figure 9. Variation of the hydrodynamic radius R_H with the reduced time under different r_{PWA}s.

homogenize the solution structures, the base-catalyzed sol−gel processing would be a better method compared to the acid-catalyzed systems for constitution of uniform polymer composite. However, PWA, playing an acid catalyst as well as a proton conductor, cannot maintain the unique polyhedral structure above pH = 2 and therefore loses its exceptional high proton conductivity. From this viewpoint, a strong acid catalyst may be a good candidate for designing proton-conducting polymer composites with uniform structures.

Conclusions

Real-time observation of the sol−gel process and subsequent cluster dilution analysis for the sol−gel-derived polymer composite, 1,8-bis(triethoxysilyl)octane (TES-Oct), containing phosphotungstic acid (PWA) have been conducted by dynamic light scattering (DLS). The two relaxation modes were observed in the time−intensity correlation function and were assigned to the cooperative diffusion in semidilute solutions and the translational diffusion of cross-linked clusters in the concentrated matrix. These modes were successfully analyzed by a combination function of a single-exponential function and a stretched exponential function of the reaction time. A quantitative evaluation of the strength of the fast mode and averaged relaxation time for the slow mode provided information on the gelation mechanism. As a result, exceptionally larger values of A_f and $\langle\tau_{slow}\rangle$ were found during the gelation around r_{PWA} = 0.100. To clarify the detail reaction mechanism, other spectroscopic methods such as FTIR and NMR techniques are strongly desired. Though such kinds of experiments have not been carried out in this study, the cluster size evolution was examined by diluting the sample at several sampling points instead. As a result, the dilution analysis for quenched samples obtained at several sampling points also supports the above findings. Because further introduction of PWA leads to the phase separation, there exists an optimal concentration of PWA for the formation of a uniform structure. To design a polymer composite with higher proton conductivity, shifting this optimal value to higher PWA concentration is demanded. This purpose may be achieved by a better choice of the precursor and the experimental conditions, such as varying the length of the organic bridging groups, the type of functional groups, the amount of water, and so on.

Acknowledgment. This work is supported by the Grant-in-Aid No. 13750832 from the Ministry of Education, Science, Sports, Culture, and Technology, Japan. We thank Dr. H. Urakawa in KIT to use the DLS apparatus.

References and Notes

(1) Shea, K. J.; Loy, D. A. *Chem. Mater.* **2001**, *13*, 3306.
(2) Fan, H.; Reed, S.; Baer, T.; Schunk, R.; Lopez, G. P.; Brinker, C. J. *Microporous Mesoporous Mater.* **2001**, *44*−*45*, 625.
(3) Corriu, R. J. P.; Moreau, J. J. E.; Thepot, P.; Man, M. W. C. *Chem. Mater.* **1996**, *8*, 100.
(4) Loy, D. A.; Beach, J. V.; Baugher, B. M.; Assink, R. A. *Chem. Mater.* **1999**, *11*, 3333.
(5) Dahmouche, K.; Santilli, C. V.; Pulcineli, S. H.; Craievich, A. F. *J. Phys. Chem. B* **1999**, *103*, 4937.
(6) Honma, I.; Nomura, S.; Nakajima, H. *J. Membr. Sci.* **2001**, *185*, 83.
(7) Lavrencic Stangar, U.; Groselj, N.; Orel, B.; Colomban, P. *Chem. Mater.* **2000**, *12*, 3745.
(8) *Heteropoly and Isopoly Oxometalates*; Pope, M. T., Ed.; Springer-Verlag: Berlin, 1983.
(9) *Metal*−*Oxygen Clusters: The Surface and Catalytic Properties of Heteropoly Oxometalates*; Moffat, J. B., Ed.; Kluwer Academic/Plenum Publishers: New York, 2001.
(10) Mohapatra, S. K.; Boyd, G. D.; Storz, F. G.; Wagner, S. *J. Electrochem. Soc.* **1979**, *126*, 805.
(11) Dahmouche, K.; Carlos, L. D.; Santilli, C. V.; de Zea Bermudez, V.; Craievich, A. F. *J. Phys. Chem. B* **2002**, *106*, 4377.
(12) Jiang, S.; Xia, K.-Q.; Xu, G. *Macromolecules* **2001**, *34*, 7783.
(13) Kanao, M.; Matsuda, Y.; Sato, T. *Macromolecules* **2003**, *36*, 2093.
(14) Joosten, J. G. H.; McCarthy, J. L.; Pusey, P. N. *Macromolecules* **1991**, *24*, 6690.
(15) Rouf-George, C.; Munch, J.-P.; Schosseler, F.; Pouchelon, A.; Beinert, G.; Boue, F.; Bastide, J. *Macromolecules* **1997**, *30*, 8344.
(16) Shibayama, M. *Macromol. Chem. Phys.* **1998**, *199*, 1.
(17) Zhao, Y.; Zhang, G.; Wu, C. *Macromolecules* **2001**, *34*, 7404.
(18) Hecht, A. M.; Horkay, F. H.; Schleger, P.; Geissler, E. *Macromolecules* **2002**, *35*, 8552.
(19) Aymard, P.; Durand, D.; Nicolai, T. *Int. J. Polym. Anal. Charact.* **1996**, *2*, 115.
(20) Gimel, J. C.; Durand, D.; Nicolai, T. *Macromolecules* **1994**, *25*, 583.
(21) Papadakis, C. M.; Almdal, K.; Mortensen, K.; Rittig, F.; Fleischer, G.; Stepanek, P. *Eur. Phys. J. E* **2000**, 275.
(22) Norisuye, T.; Inoue, M.; Shibayama, M.; Tamaki, R.; Chujo, Y. *Macromolecules* **2000**, *33*, 500.
(23) Mioc, U. B.; Dimitrijevic, R. Z.; Davidovic, M.; Nedic, Z. P.; Mitrovic, M. M.; Colomban, P. *J. Mater. Sci.* **1994**, *29*, 3705.
(24) Nakanishi, T.; Norisuye, T.; Tran-Cong-Miyata, Q.; Nomura, S.; Sugimoto, T., manuscript in preparation.
(25) *Dynamic Light Scattering, the Methods and Applications*; Brown, W., Ed.; Clarendon Press: Oxford, 1993.
(26) Berne, B. J.; Pecora, R. *Dynamic Light Scattering with Applications to Chemistry, Biology and Physics*; Dover Publications: Mineola, NY, 2000.
(27) Brochard, F.; de Gennes, P. G. *Macromolecules* **1977**, *10*, 1157.
(28) Adam, M.; Delsanti, M. *Macromolecules* **1985**, *9*, 1760.
(29) Doi, M.; Onuki, A. *J. Phys. II* **1992**, *2*, 1631.
(30) Stepanek, P. *Macromolecules* **1998**, *31*, 1889.
(31) Einaga, Y.; Karube, D. *Polymer* **1999**, 157.
(32) Heckmeier, M.; Mix, M.; Strobl, G. *Macromolecules* **1997**, *30*, 4454.
(33) Martin, J. E.; Wilcoxon, J.; Odinek, J. *Phys. Rev. A* **1991**, *43*, 858.

(34) Adam, M.; Delsanti, M.; Munch, J. P.; Durand, D. *Phys. Rev. Lett.* **1988**, *61*, 706.
(35) Lesturgeon, V.; Nicolai, T.; Durand, D. *Eur. Phys. J. B* **1999**, *9*, 71.
(36) Kita, R.; Takahashi, A.; Kaibara, M.; Kubota, K. *Biomacromolecules* **2002**, *3*, 1013.
(37) Shibayama, M.; Norisuye, T. *Bull. Chem. Soc. Jpn.* **2002**, *75*, 641.
(38) Adam, M.; Lairez, D. In *Physical Properties of Polymeric Gels*; Cohen Addad, J. P., Ed.; John Wiley & Sons: New York, 1996; p 87.
(39) Norisuye, T.; Shibayama, M.; Nomura, S. *Polymer* **1998**, *39*, 2769.
(40) Okamoto, M.; Norisuye, T.; Shibayama, M. *Macromolecules* **2001**, *34*, 8496.
(41) Brinker, C. J.; Scherer, G. W. *J. Non-Cryst. Solids* **1985**, *70*, 301.
(42) Brinker, C. J.; Scherer, G. W. *Sol−Gel Science*; Academic Press: London, 1990.

MA034987B